ACS OMEGA

Article

Cite This: ACS Omega 2019, 4, 14040−14048

http://pubs.acs.org/journal/acsodf

Probing the Reactivity of Singlet Oxygen with Cyclic Monoterpenes

Nassim Zeinali,[†] Ibukun Oluwoye,[†] Mohammednoor K. Altarawneh,*[,†,‡] Mansour H. Almatarneh,*[,§] and Bogdan Z. Dlugogorski[∥]

[†]Discipline of Chemistry and Physics, College of Science, Health, Engineering and Education, Murdoch University, Murdoch, WA 6150, Australia

[‡]Chemical Engineering Department, UAE University, Al-Ain 15551, United Arab Emirates

[§]Department of Chemistry, University of Jordan, Amman 11942, Jordan

[∥]Office of Deputy Vice Chancellor Research & Innovation, Charles Darwin University, Darwin, NT 0909, Australia

ABSTRACT: Monoterpenes represent a class of hydrocarbons consisting of two isoprene units. Like many other terpenes, monoterpenes emerge mainly from vegetation, indicating their significance in both atmospheric chemistry and pharmaceutical and food industries. The atmospheric recycling of monoterpenes constitutes a major source of secondary organic aerosols. Therefore, this contribution focuses on the mechanism and kinetics of atmospheric oxidation of five dominant monoterpenes (i.e., limonene, α-pinene, β-pinene, sabinene, and camphene) by singlet oxygen. The reactions are initiated via the ene-type addition of singlet oxygen (O_2 $^1\Delta_g$) to the electron-rich double bond, progressing favorably through the concerted reaction mechanisms. The physical analyses of the frontier molecular orbitals agree well with the thermodynamic properties of the selected reagents, and the computed reaction rate parameters. The reactivity of monoterpenes with O_2 $^1\Delta_g$ follows the order of α-pinene > sabinene > limonene > β-pinene > camphene, i.e., α-pinene and camphene retain the highest and lowest reactivity toward singlet oxygen, with rate expressions of $k(T)$ (M^{-1} s^{-1}) = $1.13 \times 10^8 \exp(-48(\text{kJ})/RT(\text{K}))$ and $6.93 \times 10^8 \exp(-139(\text{kJ})/RT(\text{K}))$, respectively. The effect of solvent on the primary reaction pathways triggers a slight reduction in energy, ranging between 12 and 34 kJ/mol.

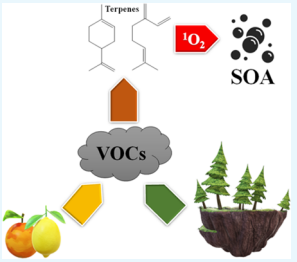

1. INTRODUCTION

Plants emit nearly 98% of the total non-methane volatile organic compounds into the atmosphere, 20% of which comprises monoterpenes.[1] Monoterpenes represent a class of C_{10} members of terpene hydrocarbons, the biogenic (naturally occurring) volatile organic compounds (BVOC) with high chemical reactivity and annual global emission rate of between 128 and 450 Tg per year.[2] Figure 1 summarizes the photosensitised oxidation products of the selected monoterpenes detected and characterized in literature.[3−7] The chemical structure of monoterpenes features two isoprene units, constituting the major component of essential oils in various plant matters and can be isolated from trees for anti-inflammatory and antimicrobial drug synthesis.[8] An alternative source of monoterpene emission includes woody household products.[9]

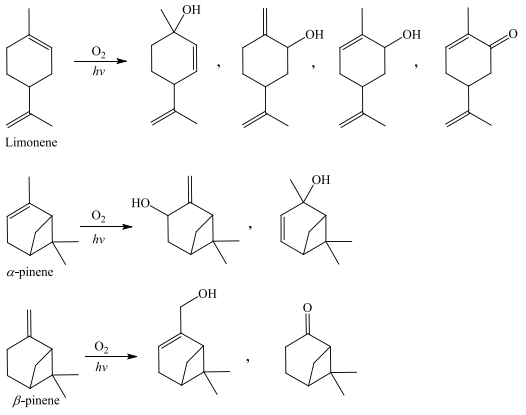

Figure 1. Oxidation products of limonene, α-pinene, and β-pinene by O_2 $^1\Delta_g$.[3−7]

Limonene and pinene are among the most abundant monoterpenes operating in the global tropospheric chemistry,[10,11] being produced in relatively noticeable quantities by vegetation such as aromatic plants, flowers, and leaves. Limonene arises mainly from young plant leaves, and its formation rate reduces rapidly based on the age and extent of oxidation of the leaves.[12] Moreover, this monocyclic monoterpene is significantly utilized in medicinal chemistry and disease treatment, due to its antitumor and antibacterial activity, and dietary formulations.[13,14] Over 80% of the total monoterpene emission from a Monterey pine (*Pinus radiata*) comprises α- and β-pinene,[15] and it has also been evidenced that about 50% of the emitted monoterpene from forests and tree species in the United States consists of α-pinene.[16] Other examples of bicyclic monoterpenes are camphene and sabinene, which are minor constituents of many essential oils from plants such as turpentine, rosemary, ginger, and valerian.

Received: June 19, 2019
Accepted: July 18, 2019
Published: August 14, 2019

DOI: 10.1021/acsomega.9b01825
ACS Omega 2019, 4, 14040−14048

Tropospheric hydrocarbons such as monoterpenes have relatively high molecular weights, thus their atmospheric oxidation gives rise to semivolatile organic compounds and secondary organic aerosol (SOA). SOAs originate primarily from the oxidation of BVOCs including monoterpenes. Subsequently, SOA plays a significant part in climate change and global radiation imbalance due to their involvement in the absorption and scattering of solar radiation. For instance, SOA are significant constituents of atmospheric fine particulate matters (PM2.5) as well as various haze pollution episodes.[17] Monoterpenes find further applications in aromatization of cleaning products, paintings, air fresheners, and flavoring agents due to their pleasant fragrance. Therefore, the risk of accumulation of atmospheric oxidation products (i.e., SOA) could be substantial in enclosed, poorly ventilated spaces.

The maximum rate of singlet O_2 formation by energy-transfer mechanism in a polluted atmosphere is approximated to be 4×10^{-12} mol L^{-1} s^{-1}, which corroborates the significant role of such reactive oxygen species as atmospheric oxidants.[18] Reactions of singlet oxygen with electron-rich acceptors such as olefins, dienes, and aromatic compounds are grouped into [4 + 2]-cycloadditions, [2 + 2]-cycloadditions, and the so-called ene reactions. Ene reaction is based on the interaction of $^1O_2$ with an unsaturated compound containing an allylic hydrogen, during which the allylic hydrogen is abstracted in association with a reorganization of the bonding to give allylhydroperoxides.[19] Oxidation of substrates with conjugated double bonds by singlet oxygen is feasible through [4 + 2]-cycloaddition, resulting in the synthesis of endoperoxides. Furthermore, the [2 + 2]-cycloaddition of the singlet oxygen to one double bond results in 1,2-dioxetane, and apparently olefins with unreachable allylic hydrogen atoms tend to give [2 + 2]-adducts.[20] However, it should be noted that all of the reactions can compete for the same substance if the molecular structure allows it.[21]

Previous research efforts had investigated the oxidation of monoterpenes to SOA by OH radical,[22,23] ozone,[24−26] hydrogen peroxide,[27−29] and nitrogen oxides,[30−32] reporting the yield of the corresponding carbonyl compounds as the predominant products as a result of the oxidative cleavage of the C=C bonds.[33] However, the role of a highly reactive singlet molecular oxygen in the photo-oxidation of monoterpenes has not been properly addressed in the literature. Some experimental studies elucidating the product distribution of dye-sensitized oxidation of terpenoid biogenic hydrocarbons (i.e., limonene, α-, and β-pinene) in different media demonstrated the formation of organic aerosols.[3,4,34,35] The aim of this contribution is to report modes of reactions between singlet oxygen and monoterpenes with a prime focus on deriving kinetic parameters.

2. RESULTS AND DISCUSSION

2.1. Mechanism and Kinetics of Singlet Oxidation of Monoterpenes. Due to the extreme electrophilic nature of singlet oxygen, the introduction of oxygen atoms into monoterpenes during photo-oxidation will occur at the molecular site where the Fukui function for an electrophilic attack (f^{-1}) displays its maximum value. This parameter indicates the most reactive site of chemical systems for electrophilic substitution reactions. According to Figure 2, the f^{-1} indices are the largest at >C=C< sites associated with the higher photo-oxidation reactivity of nucleophile substrates therein.

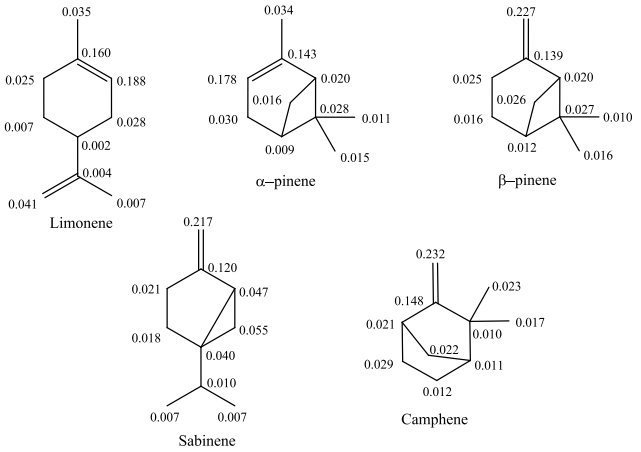

Figure 2. Local electrophilic Fukui indices (f^{-1}) of reactive monoterpenes.

The interaction between the nucleophile's HOMO and the electrophile's LUMO plays a vital role in elucidating the reaction dynamics, as though the larger LUMO−HOMO energy gaps lead to the decelerated chemical reactivity. E_{HOMO} for selected monoterpenes and E_{LUMO} for singlet oxygen are shown in Figure 3. Apparently, α-pinene appears to be most

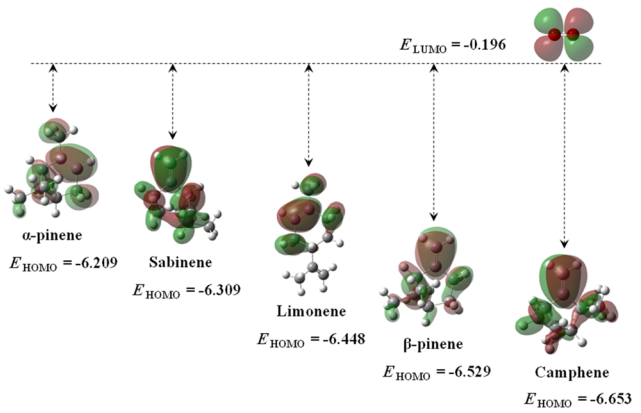

Figure 3. Electron cloud distribution and energy levels of HOMO of monoterpenes and LUMO of singlet oxygen. Energy values are in eV unit.

reactive toward singlet oxygen, whereas camphene exhibits the least reactivity among all. Based on the electron cloud distribution in Figure 3, the valence orbital electrons highly engulf the π-bond, justifying the Fukui indices results (Figure 2) to designate >C=C< as the most favorable molecular site for electrophilic attacks.

Table 1 lists the global hardness (η), softness (S), electronegativity (χ), chemical potential (μ), and electrophilicity index (ω) of the species derived from the computed HOMO and LUMO energy levels, enabling the predictions of the respective chemical characteristics of the species. Camphene remains the hardest reagent with the highest electronegativity and the lowest chemical potential. Apparently, the higher electronegativity signifies the lower chemical activity, all of which connote a higher oxidation resistance.[36] Thus, the following trend of chemical reactivity of the species is predicted herein: α-pinene > sabinene > limonene > β-pinene > camphene. The stated reactivity sequence accords well with the arrangement of the energy gap between LUMO

DOI: 10.1021/acsomega.9b01825
ACS Omega 2019, 4, 14040−14048

Table 1. HOMO/LUMO Energies, Electronegativities (χ), Hardnesses (η), Softness (S), and Electrophilicity Index (ω) of the Monoterpene Species Obtained at the B3LYP 6-311+g(d,p) Level of Calculations[a]

	E_{HOMO}	E_{LUMO}	$\Delta E_{LUMO-HOMO}$	χ	μ	η	S	ω
limonene	−6.448	−0.055	6.393	3.252	−3.252	3.196	0.313	1.654
α-pinene	−6.209	0.017	6.226	3.096	−3.096	3.113	0.321	1.540
β-pinene	−6.529	0.005	6.534	3.262	−3.262	3.267	0.306	1.628
camphene	−6.653	−0.007	6.646	3.330	−3.330	3.323	0.301	1.669
sabinene	−6.309	−0.063	6.246	3.186	−3.186	3.123	0.320	1.625

[a]Values are in eV.

of O_2 $^1\Delta_g$ and HOMO of monoterpene species in Figure 3, i.e., the smaller the energy gap, the higher the reactivity.

The following sections present the mechanisms of reaction of each of the aforementioned monoterpenes with singlet oxygen, discussing in detail the energy potentials and kinetics features of the reactions.

2.1.1. Limonene. Figure 4 displays the optimized structure of limonene. According to the acquired reactivity indices in

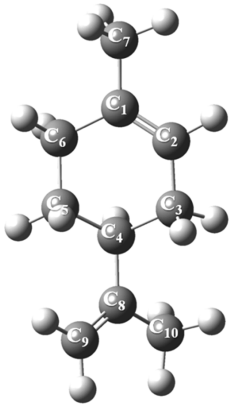

Figure 4. Optimized structure of limonene computed at the B3LYP/6-311+g(d,p) level of theory.

Figure 2, the most vulnerable site for electrophilic attack rests on the trisubstituted double bond (C_1═C_2). Therefore, the plausible reaction mechanisms for singlet oxidation of limonene should involve the ene reaction and [2 + 2]-cycloaddition. The latter failed to locate a genuine transition state despite our best efforts. Thus, the overall reaction merely involves ene-type reaction of O_2 $^1\Delta_g$ with limonene's unconjugated double bond to form allylic hydroperoxides. Yet, our computational model failed to optimize related diradicals as potential intermediates in the ene reactions of limonene photo-oxidation, prompting to suggest a concerted mechanism for the ene-type addition of singlet oxygen to the limonene structure.

As illustrated in the proposed reaction mechanism in Figure 5, singlet oxygen clings to the limonene's cyclohexene ring at the C_2 atom, bearing analogous barrier enthalpies of TS_2 and TS_3 around 40 kJ/mol. Hydrogen abstraction from the methylene group (in P_3) appears relatively energetically more favorable as compared to that from the methyl group (in P_2). The C_1 atom represents an alternative reactive spot for the addition of singlet oxygen enduring a relatively higher enthalpy barrier of TS_1 (50 kJ/mol). In accordance to the computed Fukui indices in Figure 2, this enthalpic behavior is justifiable as the C_2 position is the most favorable site for an electrophilic attack.

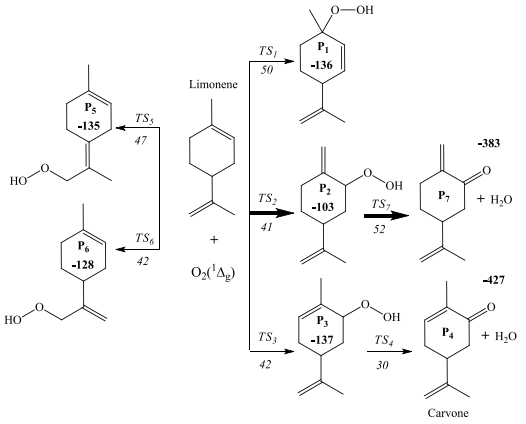

Figure 5. Reaction mechanism of the singlet oxidation of limonene. The enthalpies are obtained at the 6-311+g(d,p) level of theory and are reported in kJ/mol.

Although the electrophilic Fukui functions demonstrate that the likelihood of the C_8═C_9 site to be attacked by electrophiles is negligible, the corresponding transition state values (TS_5 and TS_6) compare well with the transition states for the attack on the C_1═C_2 in-ring double bond. As previously illustrated in Figure 1, the literature suggests that the product distribution from the photo-oxidation of limonene consists of terpene alcohols that are being reduced from P_1, P_2, and P_3 hydroperoxides, whose RO−OH bond efficiently undergoes a cleavage. Table 2 lists the reaction rate coefficient

Table 2. Kinetic Parameters of Limonene Interaction with O_2 $^1\Delta_g$

reaction	A (s^{-1} or cm^3 $molecule^{-1}$ s^{-1})	E_a (kJ/mol)
limonene + O_2 $^1\Delta_g$ → P_1	1.53×10^{-13}	57
limonene + O_2 $^1\Delta_g$ → P_2	1.87×10^{-13}	48
limonene + O_2 $^1\Delta_g$ → P_3	9.71×10^{-13}	49
limonene + O_2 $^1\Delta_g$ → P_5	3.43×10^{-13}	54
limonene + O_2 $^1\Delta_g$ → P_6	2.25×10^{-13}	49

for the bimolecular reactions involved in the interaction of limonene with the singlet oxygen, fitted to the Arrhenius equation of $k(T) = Ae^{-E_a/RT}$ at a high pressure limit for the temperature range of 300 and 600 K.

The branching ratios for the bimolecular reaction channels are evaluated based on the Arrhenius parameters for $k_i(T)$ given in Table 2. Figure 6 plots the $k_i/\sum k_i$, verifying channel TS_3 as the dominant reaction pathway and P_3 as the major primary product according to the reaction network. In a qualitative agreement with the experimental results by Chalchat et al.,[37] P_3 constituted ∼40% of the initial product yield from the photochemical hydroperoxidation of limonene

DOI: 10.1021/acsomega.9b01825
ACS Omega 2019, 4, 14040−14048

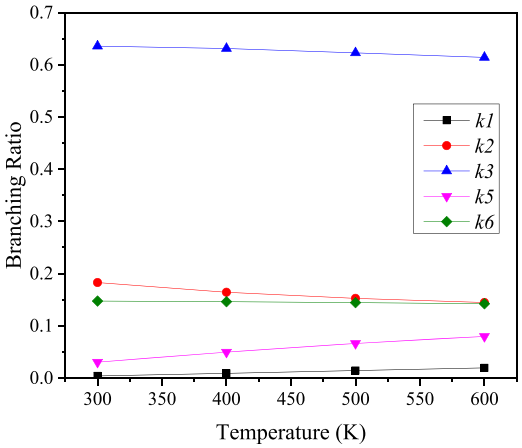

Figure 6. Plot of branching ratios of different reaction pathways as a function of temperature (K).

in the presence of oxygen. In general, photo-oxidation of the products of limonene features −OOH/−OH/−O substitution at para position.[7,37] This is consistent with our prediction of P_3 as the likely dominant initial intermediate.

A subsequent H-transfer step into the outer OH group in the P_3 intermediate liberates a water molecule and forms the experimentally detected product of carvone (P_4) via an accessible energy barrier of only 30 kJ/mol.

In addition to carvone, terpene alcohols constitute the major experimentally detected products from the photo-oxidation of limonene. As illustrated above, these molecules most likely arise from a radical-induced mechanism that begins with the fission of the O−OH bonds in the P_1−P_6 intermediates. For instance, the four para-substituted terpene alcohols account for 60% of the total product yields from the photo-oxidation of limonene.[37] Clearly, these compounds may originate from the scission of the O−OH bond in the predicted dominant P_3 intermediate followed by H abstraction by the phenoxy-type O atom and structural arrangements. Products feature ipso substitution, most likely directly stemming from the P_1 moiety or via an intramolecular transfer of the OOH group along the reaction $P_3 \rightarrow P_1$. Such a step proceeds without encountering a reaction as an intrinsic barrier in a thermodynamically neutral reaction.

2.1.2. Pinene. Figures 7,8, and 9 depict the optimized structures of α- and β-pinene. The f^{-1} indices (Figure 2) reveal

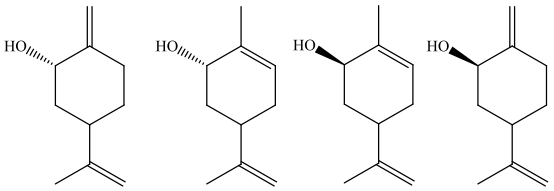

Figure 7. Structures of para-substituted terpene alcohols.

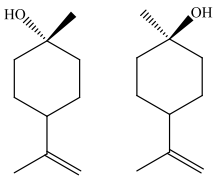

Figure 8. Structures of ipso-substituted terpene alcohols.

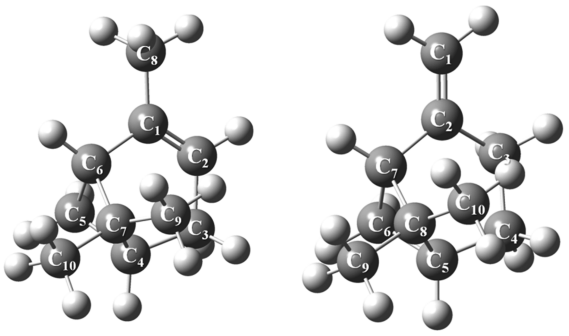

Figure 9. Optimized structures of α-pinene (left) and β-pinene (right) computed at B3LYP/6-311+g(d,p) level of theory.

C_2 in α-pinene and C_1 in β-pinene structures as the most preferred sites of interaction with electrophilic species. We were unable to locate the transition structures for the [2 + 2]-cycloaddition of singlet oxygen to pinene, certifying that the formation of hydroperoxides as the sole light-induced oxidation product of α- and β-pinene stems from ene-type reaction.[38,39]

The reaction mechanisms of the singlet oxidation of α- and β-pinene are displayed in Figures 10 and 11, respectively. The

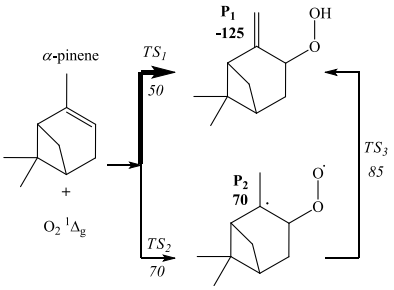

Figure 10. Reaction mechanism of the singlet oxidation of α-pinene. The enthalpies are obtained at the 6-311+g(d,p) level of theory and are in kJ/mol.

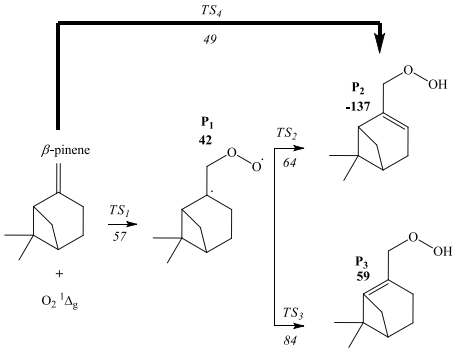

Figure 11. Reaction mechanism of the singlet oxidation of β-pinene. The enthalpies are obtained at the 6-311+g(d,p) level of theory and are in kJ/mol.

figures reveal that the ene reaction proceeds with the addition of singlet oxygen to the in-ring C_2 atom of α-pinene and the abstraction of allylic hydrogen from the methyl group via concerted or stepwise mechanisms. The stepwise TS_2 barrier overshoots the concerted TS_1 by 20 kJ/mol, leaving the concerted mechanism as the dominating reaction pathway for the formation of P_1 hydroperoxide. The product P_1 is also

DOI: 10.1021/acsomega.9b01825
ACS Omega 2019, 4, 14040−14048

attainable through a stepwise channel via a facile transformation of the diradical (P_2) to hydroperoxide (P_1).[40] Jefford et al.[4] recorded similar observation, identifying P_1 as the utmost product from the $^1O_2$-initiated atmospheric oxidation of α-pinene.

Moreover, as shown in Figure 11, the ene-type addition of the singlet oxygen to C_1 atom within a β-pinene structure (the one with the highest Fukui function value) occurs similarly in both stepwise and concerted fashions through TS_1 (57 kJ/mol) and TS_4 (49 kJ/mol) steps. Apparently, the concerted mechanism (TS_4) is the governing reaction channel triggering the formation of P_2 hydroperoxide as the major product of the singlet oxidation of β-pinene. The stepwise TS_1 channel, on the other hand, gives rise to the production of a diradical P_1, which further branches into two exit routes, resulting in two types of hydroperoxide adducts, P_2 and P_3. The product P_2 resides in a significant well-depth in reference to the entrance channel, affirming its greater stability as compared to P_3 hydroperoxide. Besides, TS_2 signifies a trivial transition barrier leading to the formation of the main product P_2.

Table 3 presents the fitted Arrhenius parameters. According to the computed reaction rate coefficients, the α-pinene + O_2 $^1\Delta_g$ reaction proceeds predominantly by the ene addition of the singlet delta oxygen to C_2 atom to form P_1 hydroperoxide in a concerted mechanism. Oxidation of β-pinene by $^1O_2$ similarly proceeds through a concerted channel, giving rise to the formation of P_2 hydroperoxide via an enthalpy barrier of 49 kJ/mol.

Table 3. Kinetic Parameters of α- and β-Pinene Interaction with O_2 $^1\Delta_g$

reaction	A (s^{-1} or cm^3 $molecule^{-1}$ s^{-1})	E_a (kJ/mol)
α-pinene + O_2 $^1\Delta_g$ → P_1	2.51×10^{-13}	57
α-pinene + O_2 $^1\Delta_g$ → P_2	3.50×10^{-13}	63
P_2 → P_1	$3.19 \times 10^{+12}$	12
β-pinene + O_2 $^1\Delta_g$ → P_1	1.18×10^{-12}	64
P_1 → P_2	$2.93 \times 10^{+12}$	25
P_1 → P_3	$1.16 \times 10^{+12}$	45
β-pinene + O_2 $^1\Delta_g$ → P_3	2.99×10^{-13}	56

Data in Table 3 afforded the estimation of the branching ratios of the bimolecular reaction channels for α- and β-pinene as shown in Figure 12. In view of this finding, the concerted TS_1 channel remains the dominant reaction pathway for the singlet oxidation of α-pinene, and there exists a moderate decline in the branching ratio value as the temperature increases, reflecting the reverse effect of temperature on the reaction rate constant of the concerted mechanism of the singlet oxygen addition to α-pinene.

In a similar fashion, the concerted TS_4 step leads to the reaction pathways for the singlet oxidation of β-pinene and the calculated branching ratios show that the contribution of the concerted mechanism (k_4) noticeably diminishes as the temperature increases. Nonetheless, at atmospheric relevant temperatures (i.e., 300 K), reaction of β-pinene with singlet oxygen largely ensues via the concerted mechanism.

2.1.3. Camphene and Sabinene. There exists a resemblance between the structure of camphene (Figure 13) and β-pinene owing to the presence of an exocyclic double bond. Therefore, the addition of a singlet oxygen to camphene in an ene reaction mode occurs at the C_1 position via a stepwise mechanism.

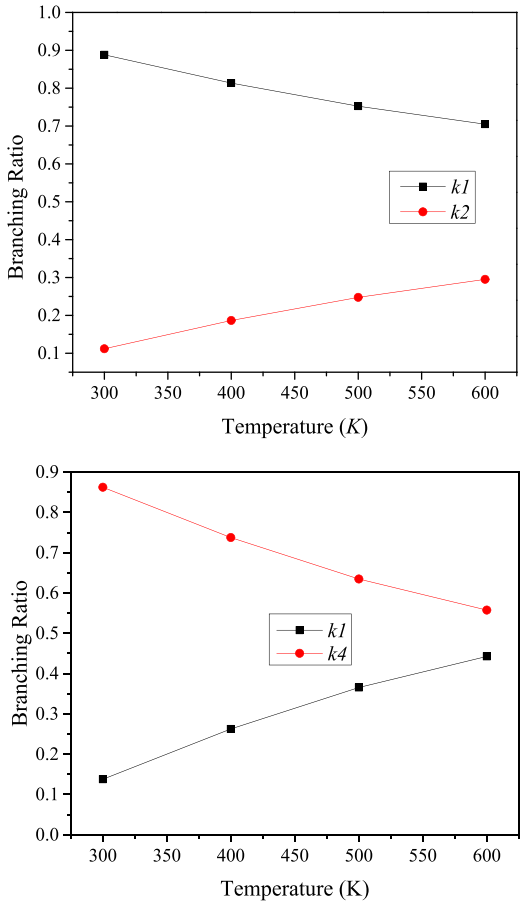

Figure 12. Plots of branching ratios of α-pinene (top) and β-pinene (bottom) at different temperatures (K).

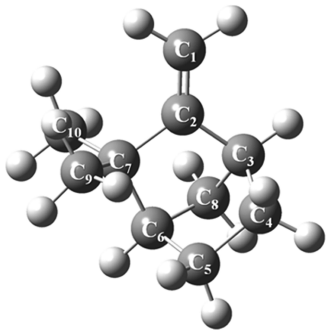

Figure 13. Optimized structure of camphene computed at the B3LYP/6-311+g(d,p) level of theory.

According to the mechanism of the singlet-oxygen-initiated atmospheric oxidation of camphene shown in Figure 14, the initial reaction between camphene and singlet oxygen

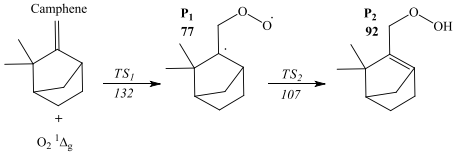

Figure 14. Reaction mechanism of the singlet oxidation of camphene. The enthalpies are obtained at the 6-311+g(d,p) level of theory and are in kJ/mol.

DOI: 10.1021/acsomega.9b01825
ACS Omega 2019, 4, 14040−14048

comprises $O_2\ ^1\Delta_g$ addition to the terminal carbon atom of C_1 via sizable thermal enthalpy (TS_1) amounting to 132 kJ/mol. The resulting highly unstable diradical (P_2) is then transformed to the P_2 hydroperoxide adduct through a readily accessible transition state TS_2 through an enthalpic barrier of 30 kJ/mol.

Table 4 assembles the fitted high-pressure limiting Arrhenius parameters. The relatively high activation barrier of camphene

Table 4. Arrhenius Parameters for Camphene Oxidation by Singlet Oxygen

reaction	A (s^{-1} or cm^3 $molecule^{-1}$ s^{-1})	E_a (kJ/mol)
camphene + $O_2\ ^1\Delta_g \rightarrow P_1$	1.15×10^{-12}	139
$P_1 \rightarrow P_2$	$3.58 \times 10^{+12}$	33

photo-oxidation (E_a = 139 kJ/mol) correlates well with its high LUMO−HOMO energy gap (Table 1) and proves its slight tendency to undergo $^1O_2$-induced oxidation process.

Furthermore, sabinene, as illustrated in Figure 15, represents a bicyclic monoterpene and encompasses an exocyclic double

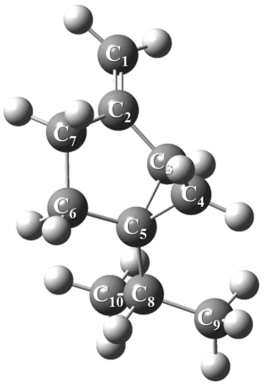

Figure 15. Optimized structure of sabinene computed at the B3LYP/6-311+g(d,p) level of theory.

bond. The sabinene's terminal double bond is characterized as an exclusive electron-rich molecular site and could readily be attacked by reactive oxygen species such as $O_2\ ^1\Delta_g$.

Introduction of singlet oxygen to the sabinene structure via ene reaction takes place at the C_1 site through a concerted bimolecular reaction bearing a slight thermal enthalpy barrier of 55 kJ/mol (Figure 16). The oxidation process proceeds with an activation energy of 62 kJ/mol as obtained from the first-order Arrhenius equation fitted for the temperature range of 300−600 K (Table 5).

The resulting hydroperoxide (P_1) would presumably be reduced to the corresponding alcohol (I) and aldehyde (II) via

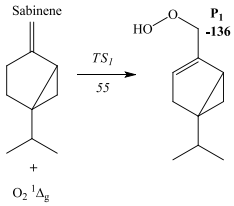

Figure 16. Reaction mechanism of the singlet oxidation of sabinene. The enthalpies are obtained at the 6-311+g(d,p) level of theory and are in kJ/mol.

Table 5. Arrhenius Parameters for Sabinene Oxidation by Singlet Oxygen

reaction	A (s^{-1} or cm^3 $molecule^{-1}$ s^{-1})	E_a (kJ/mol)
sabinene + $O_2\ ^1\Delta_g \rightarrow P_1$	5.12×10^{-13}	62

the O−O bond fission stimulated by thermal or catalytic effects.[41]

2.2. Effect of Solvent on Singlet Oxidation of Cyclic Monoterpenes. This section considers the influence of solvent in the relevant process involving the interaction of singlet oxygen with monoterpenes rather than atmospheric oxidation. The selected monoterpenes are nearly insoluble in water[42] and thus methanol served as the solvent herein. The polarizable continuum model[43] simulates the aqueous medium. In essence, this method relies on the representation of a solute molecule as a charge distributor located inside a cavity surrounded by a continuous dielectric medium, which is polarized as a result of the point charge distribution on the cavity surface.

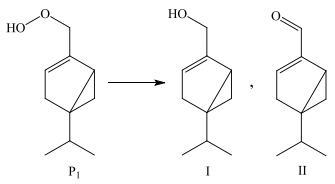

Figure 17. Reduction of hydroperoxide to terpene alcohol and aldehyde.

According to Figures 17 and 18, the effect of solvent is revealed through a systematic energy reduction in the barrier enthalpies of the transition states, intermediates, and final products along the major channels of the singlet oxygen interaction with each monoterpene substrate. The reduced enthalpies (involving solvent effect) with reference to the gas-phase system range from 12 kJ/mol (P_1 value in α-pinene) to 34 kJ/mol (P_7 value in limonene). Although the reaction barrier enthalpies are influenced by solvent effects, the product distribution and reaction channels remain intact.

3. CONCLUSIONS

Introduction of singlet oxygen to the cyclic monoterpenes exclusively follows the ene reaction pathway to yield the corresponding allylic hydroperoxides. Limonene and sabinene photo-oxidation transpire through concerted mechanisms, whereas singlet oxidation of β-pinene and camphene proceed via stepwise mechanism, resulting in the formation of diradical intermediates. In the case of α-pinene, the concerted channel ensues the most energetically favorable pathway. In terms of reactivity, α-pinene and sabinene exhibit the highest reactivity, while camphene is kinetically evidenced to be the lowest reactive species incurring relatively high activation energy of 139 kJ/mol.

4. METHODOLOGY

Gaussian 09 program[44] deployed the unrestricted density functional theory in acquiring optimized energies and geometries of the reacting species due to its accuracy in computing singlet biradical properties.[45,46] For that reason, we utilize the B3LYP functional with the extended 6-311+g(d,p)[47] basis set.

DOI: 10.1021/acsomega.9b01825
ACS Omega 2019, 4, 14040−14048

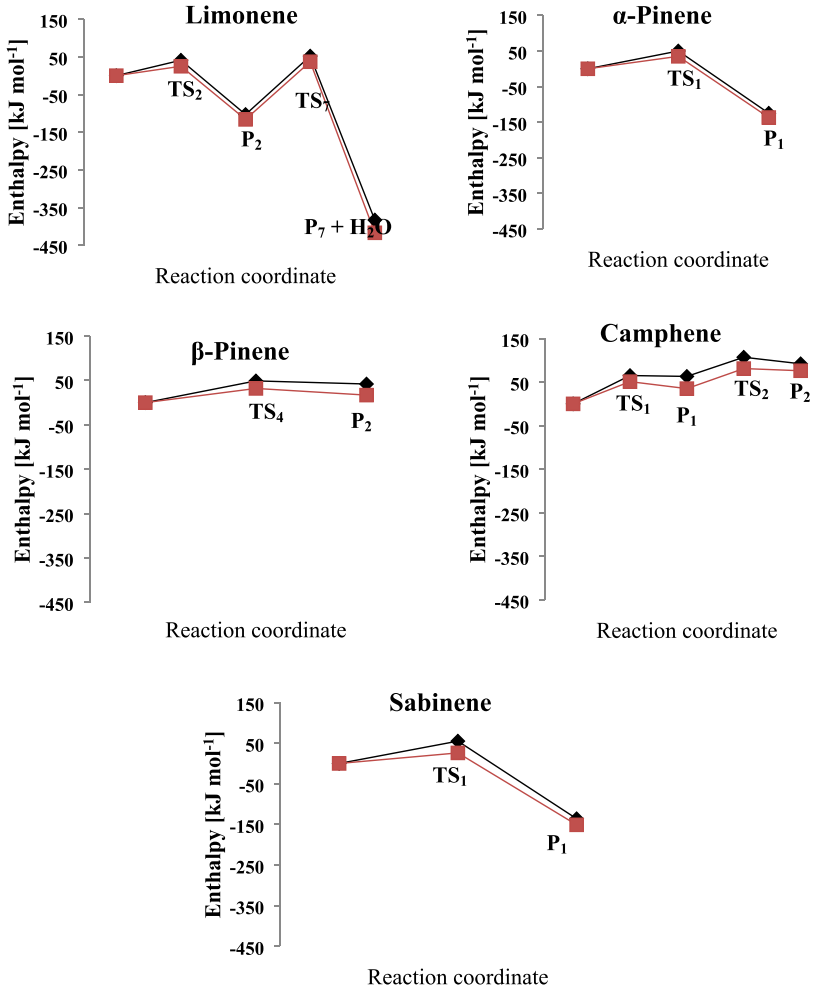

Figure 18. Potential energy diagrams of major monoterpenes + O_2 $^1\Delta_g$ reaction with (red) and without (black) solvent (methanol) effects.

A simple approximate spin-projection (AP) scheme[48,49] served to correct the final energies of species displaying biradical characters. For this, the approximate spin-projected energy (E^{AP}) has been derived from the energies of the broken-symmetry (E^{BS}) and pure high-spin (E^{HS}) states according to eq 1.

$$E^{AP} = f^{AP}E^{BS} - (f-1)E^{HS} \quad (1)$$

where f^{AP} denotes the spin-projection factor

$$f^{AP} = \frac{\langle S^2\rangle^{HS} - s(s+1)}{\langle S^2\rangle^{HS} - \langle S^2\rangle^{BS}} \quad (2)$$

and $\langle S^2\rangle^{HS}$ and $\langle S^2\rangle^{BS}$ signify the expectation values of the spin contamination pertinent to the pure high-spin and broken-symmetry states, respectively. We verified the transition structures via intrinsic reaction coordinate calculations. ChemRate software[50] facilitated the calculation of the reaction rate constants, within the temperature range of 300−600 K based on the Arrhenius equation. The electrophilic Fukui indices, serving as indicators for molecular site's reactivity toward electrophilic addition reactions, are quantified by Dmol^3 code[51] in Material Studio package at the B3LYP functional while applying a double numerical plus d-functions atomic basis set.

AUTHOR INFORMATION

Corresponding Authors

*E-mail: M.Altarawneh@Murdoch.edu.au. Phone: +61 (0)8 9360-7507.

*E-mail: m.almatarneh@ju.edu.jo.

ORCID

Ibukun Oluwoye: 0000-0002-0221-020X

Mohammednoor K. Altarawneh: 0000-0002-2832-3886

Mansour H. Almatarneh: 0000-0002-2863-6487

Bogdan Z. Dlugogorski: 0000-0001-8909-029X

Notes

The authors declare no competing financial interest.

ACKNOWLEDGMENTS

This study has been supported by grants of computing time from the National Computational Infrastructure (NCI) in Canberra and the Pawsey Supercomputing Centre (iVEC) in Perth. N.Z. acknowledges the Iraqi government for awarding PhD scholarships.

REFERENCES

(1) Guenther, A.; Geron, C.; Pierce, T.; Lamb, B.; Harley, P.; Fall, R. Natural emissions of non-methane volatile organic compounds, carbon monoxide, and oxides of nitrogen from North America. *Atmos. Environ.* **2000**, *34*, 2205−2230.

DOI: 10.1021/acsomega.9b01825
ACS Omega 2019, 4, 14040−14048

(2) Steinbrecher, R. In *Emission of VOCs from Selected European Ecosystems: The State of the Art*, The Proceedings of EUROTRAC Symposium, 1994; pp 448−454.
(3) Ohloff, G. Singlet Oxygen: A Reagent in Organic Synthesis. In *Organic Synthesis*; Elsevier, 1975; pp 481−502.
(4) Jefford, C. W.; Boschung, A. F.; Moriarty, R. M.; Rimbault, C. G.; Laffer, M. H. The Reaction of Singlet Oxygen with α-and β-Pinenes. *Helv. Chim. Acta* **1973**, *56*, 2649−2659.
(5) Goldberg, M. C.; Cunningham, K. M.; Aiken, G. R.; Weiner, E. R. The aqueous photolysis of α-pinene in solution with humic acid. *J. Contam. Hydrol.* **1992**, *9*, 79−89.
(6) Clark, B., Jr.; Jones, B.; Iacobucci, G. Characterization of the hydroperoxides derived from singlet oxygen oxidation of (+)-limonene. *Tetrahedron* **1981**, *37*, 405−409.
(7) Foote, C. S.; Wexler, S.; Ando, W. Chemistry of singlet oxygen III. Product selectivity. *Tetrahedron Lett.* **1965**, *6*, 4111−4118.
(8) Rufino, A. T.; Ribeiro, M.; Judas, F.; Salgueiro, L. G.; Lopes, M. C.; Cavaleiro, C.; Mendes, A. F. Anti-inflammatory and chondroprotective activity of (+)-α-pinene: structural and enantiomeric selectivity. *J. Nat. Prod.* **2014**, *77*, 264−269.
(9) Wolkoff, P.; Clausen, P.; Wilkins, C.; Nielsen, G. Formation of strong airway irritants in terpene/ozone mixtures. *Indoor Air* **2000**, *10*, 82−91.
(10) Almatarneh, M. H.; Elayan, I. A.; Poirier, R. A.; Altarawneh, M. The ozonolysis of cyclic monoterpenes: a computational review. *Can. J. Chem.* **2018**, *96*, 281−292.
(11) Atkinson, R. Gas-phase tropospheric chemistry of organic compounds: a review. *Atmos. Environ., Part A* **1990**, *24*, 1−41.
(12) Gershenzon, J.; McConkey, M. E.; Croteau, R. B. Regulation of monoterpene accumulation in leaves of peppermint. *Plant Physiol.* **2000**, *122*, 205−214.
(13) Hakim, I. A.; Harris, R. B.; Ritenbaugh, C. Citrus peel use is associated with reduced risk of squamous cell carcinoma of the skin. *Nutr. Cancer* **2000**, *37*, 161−168.
(14) Mukhtar, Y. M.; Adu-Frimpong, M.; Xu, X.; Yu, J. Biochemical significance of limonene and its metabolites: future prospects for designing and developing highly potent anticancer drugs. *Biosci. Rep.* **2018**, *38*, No. BSR20181253.
(15) Juuti, S.; Arey, J.; Atkinson, R. Monoterpene emission rate measurements from a Monterey pine. *J. Geophys. Res.: Atmos.* **1990**, *95*, 7515−7519.
(16) Geron, C.; Rasmussen, R.; Arnts, R. R.; Guenther, A. A review and synthesis of monoterpene speciation from forests in the United States. *Atmos. Environ.* **2000**, *34*, 1761−1781.
(17) Liu, J.; Chu, B.; Chen, T.; Liu, C.; Wang, L.; Bao, X.; He, H. Secondary organic aerosol formation from ambient air at an urban site in Beijing: effects of OH exposure and precursor concentrations. *Environ. Sci. Technol.* **2018**, *52*, 6834−6841.
(18) Pitts, J. N., Jr.; Khan, A. U.; Smith, E. B.; Wayne, R. P. Singlet oxygen in the environmental sciences. Singlet molecular oxygen and photochemical air pollution. *Environ. Sci. Technol.* **1969**, *3*, 241−247.
(19) Bayer, P.; Pérez-Ruiz, R.; Jacobi von Wangelin, A. Stereoselective Photooxidations by the Schenck Ene Reaction. *ChemPhotoChem* **2018**, *2*, 559−570.
(20) Clennan, E. L. Synthetic and mechanistic aspects of 1, 3-diene photooxidation. *Tetrahedron* **1991**, *47*, 1343−1382.
(21) Maranzana, A.; Ghigo, G.; Tonachini, G. Diradical and peroxirane pathways in the [π2+ π2] cycloaddition reactions of 1Δg dioxygen with ethene, methyl vinyl ether, and butadiene: a density functional and multireference perturbation theory study. *J. Am. Chem. Soc.* **2000**, *122*, 1414−1423.
(22) Hakola, H.; Arey, J.; Aschmann, S. M.; Atkinson, R. Product formation from the gas-phase reactions of OH radicals and O3 with a series of monoterpenes. *J. Atmos. Chem.* **1994**, *18*, 75−102.
(23) Atkinson, R. Kinetics and mechanisms of the gas-phase reactions of the hydroxyl radical with organic compounds under atmospheric conditions. *Chem. Rev.* **1986**, *86*, 69−201.
(24) Pinto, D. M.; Tiiva, P.; Miettinen, P.; Joutsensaari, J.; Kokkola, H.; Nerg, A.-M.; Laaksonen, A.; Holopainen, J. K. The effects of increasing atmospheric ozone on biogenic monoterpene profiles and the formation of secondary aerosols. *Atmos. Environ.* **2007**, *41*, 4877−4887.
(25) Johnson, D.; Rickard, A. R.; McGill, C. D.; Marston, G. The influence of orbital asymmetry on the kinetics of the gas-phase reactions of ozone with unsaturated compounds. *Phys. Chem. Chem. Phys.* **2000**, *2*, 323−328.
(26) Oliveira, R. d. M.; Bauerfeldt, G. Ozonolysis reactions of monoterpenes: a variational transition state investigation. *J. Phys. Chem. A* **2015**, *119*, 2802−2812.
(27) Carari, D. M.; da Silva, M. J. Fe (NO 3) 3-Catalyzed Monoterpene Oxidation by Hydrogen Peroxide: An Inexpensive and Environmentally Benign Oxidative Process. *Catal. Lett.* **2014**, *144*, 615−622.
(28) de Correa, C. M. Kinetics of limonene epoxidation by hydrogen peroxide on PW-Amberlite. *J. Mol. Catal. A: Chem.* **2002**, *185*, 269−277.
(29) da Silva, M. J.; Vieira, L. M.; Oliveira, A. A.; Ribeiro, M. C. Novel effect of palladium catalysts on chemoselective oxidation of β-pinene by hydrogen peroxide. *Monatsh. Chem.* **2013**, *144*, 321−326.
(30) Pandis, S. N.; Paulson, S. E.; Seinfeld, J. H.; Flagan, R. C. Aerosol formation in the photooxidation of isoprene and β-pinene. *Atmos. Environ., Part A* **1991**, *25*, 997−1008.
(31) Wildt, J.; Mentel, T.; Kiendler-Scharr, A.; Hoffmann, T.; Andres, S.; Ehn, M.; Kleist, E.; Müsgen, P.; Rohrer, F.; Rudich, Y.; et al. Suppression of new particle formation from monoterpene oxidation by NOx. *Atmos. Chem. Phys.* **2014**, *14*, 2789−2804.
(32) Atkinson, R. Kinetics and mechanisms of the gas-phase reactions of the NO3 radical with organic compounds. *J. Phys. Chem. Ref. Data* **1991**, *20*, 459−507.
(33) Hakola, H.; Arey, J.; Aschmann, S. M.; Atkinson, R. Product formation from the gas-phase reactions of OH radicals and O 3 with a series of monoterpenes. *J. Atmos. Chem.* **1994**, *18*, 75−102.
(34) Foote, C. S. Photosensitized oxygenations and the role of singlet oxygen. *Acc. Chem. Res.* **1968**, *1*, 104−110.
(35) You, K.; Yin, D.; Mao, L.; Liu, P.; Luo, H. A. Selective photosensitized oxidation and its catalytic regulation of monoterpene with molecular oxygen in different reaction media. *J. Photochem. Photobiol., A* **2011**, *217*, 321−325.
(36) Gao, Z.; Yang, Z.; Li, Y.; Deng, A.; Luo, Y.; Li, H.-W. Improving the phase stability and cycling performance of Ce 2 Ni 7-type RE−Mg−Ni alloy electrodes by high electronegativity element substitution. *Dalton Trans.* **2018**, *47*, 16453−16460.
(37) Chalchat, J.; Chiron, F.; Garry, R. P.; Lacoste, J.; Sautou, V. Photochemical hydroperoxidation of terpenes. Antimicrobial activity of α-pinene, β-pinene and limonene hydroperoxides. *J. Essent. Oil Res.* **2000**, *12*, 125−134.
(38) Kenney, R.; Fisher, G. Preparation of trans-Pinocarveol and Myrtenol. *Ind. Eng. Chem. Prod. Res. Dev.* **1973**, *12*, 317−319.
(39) Hennig, H.; Rehorek, D.; Stich, R.; Weber, L. Photocatalysis induced by light-sensitive coordination compounds. *Pure Appl. Chem.* **1990**, *62*, 1489−1494.
(40) Maranzana, A.; Ghigo, G.; Tonachini, G. The $^1\Delta_g$ Dioxygen Ene Reaction with Propene: A Density Functional and Multireference Perturbation Theory Mechanistic Study. *Chem. - Eur. J.* **2003**, *9*, 2616−2626.
(41) Davies, A. G.; Feld, R. 133. Organic peroxides. Part VI. A stereochemical investigation of the preparation and reactions of 1-phenylethyl hydroperoxide. *J. Chem. Soc.* **1956**, 665−670.
(42) Lide, D. R. *CRC Handbook of Chemistry and Physics*; CRC Press, 2004; Vol. 85.
(43) Barone, V.; Cossi, M.; Tomasi, J. A new definition of cavities for the computation of solvation free energies by the polarizable continuum model. *J. Chem. Phys.* **1997**, *107*, 3210−3221.
(44) Frisch, M. J.; Trucks, G. W.; Schlegel, H. B.; Scuseria, G. E.; Robb, M. A.; Cheeseman, J. R.; Scalmani, G.; Barone, V.; Mennucci, B.; Petersson, G. A.; et al. *Gaussian 09*, A.1; Gaussian, Inc: Wallingford, CT, 2009.

DOI: 10.1021/acsomega.9b01825
ACS Omega 2019, 4, 14040−14048

(45) Gräfenstein, J.; Cremer, D. The combination of density functional theory with multi-configuration methods−CAS-DFT. *Chem. Phys. Lett.* **2000**, *316*, 569−577.
(46) Cramer, C. J.; Thompson, J. Quantum chemical characterization of singlet and triplet didehydroindenes. *J. Phys. Chem. A* **2001**, *105*, 2091−2098.
(47) Montgomery, J. A., Jr.; Ochterski, J. W.; Petersson, G. A. A complete basis set model chemistry. IV. An improved atomic pair natural orbital method. *J. Chem. Phys.* **1994**, *101*, 5900−5909.
(48) Yamaguchi, K.; Takahara, Y.; Fueno, T.; Houk, K. Extended Hartree-Fock (EHF) theory of chemical reactions. *Theor. Chim. Acta* **1988**, *73*, 337−364.
(49) Yamaguchi, K.; Okumura, M.; Mori, W.; Maki, J.; Takada, K.; Noro, T.; Tanaka, K. Comparison between spin restricted and unrestricted post-Hartree—Fock calculations of effective exchange integrals in Ising and Heisenberg models. *Chem. Phys. Lett.* **1993**, *210*, 201−210.
(50) Mokrushin, V.; Bedanov, V.; Tsang, W.; Zachariah, M.; Knyazev, V. *ChemRate*, version 1.19; NIST: Gaithersburg, MD, 2002.
(51) Delley, B. From molecules to solids with the DMol3 approach. *J. Chem. Phys.* **2000**, *113*, 7756−7764.

DOI: 10.1021/acsomega.9b01825
ACS Omega 2019, 4, 14040−14048